Low-temperature and dynamic magnetism of highly frustrated $5d^2$ Li_4MgOsO_6 polymorphs in comparison with $5d^3$ $Li_3Mg_2OsO_6$

Gia T. Tran,[1] Phuong-Hieu T. Nguyen,[1] Charles J. Bloed,[1] Michael E. Evans,[2] Jamie A. Anczarski,[2] William P. Martin,[2] Jefferson Toro,[2] Demetrios V. Papakostas,[2] James Beare,[3] Murray N. Wilson,[3] John E. Greedan,[4,5] Graeme M. Luke,[3,6] Thomas Gredig,[7] Jeremy P. Carlo,[2,*] and Shahab Derakhshan[1,†]

[1]*Department of Chemistry and Biochemistry, California State University - Long Beach, Long Beach, California 90840, USA*
[2]*Department of Physics, Villanova University, Villanova, Pennsylvania 19085, USA*
[3]*Department of Physics and Astronomy, McMaster University, Hamilton, Ontario L8S 4M1 Canada*
[4]*Department of Chemistry and Chemical Biology, McMaster University, Hamilton, Ontario L8S 4M1 Canada*
[5]*Brockhouse Institute for Materials Research, McMaster University, Hamilton, Ontario L8S 4M1 Canada*
[6]*TRIUMF, 4004 Wesbrook Mall, Vancouver, British Columbia V6T 2A3 Canada*
[7]*Department of Physics and Astronomy, California State University - Long Beach, Long Beach, California 90840, USA*

(Received 12 September 2018; published 1 November 2018)

Geometric magnetic frustration has attracted substantial interest due to the exotic physics and rich phase diagrams revealed by the cancellation of normally dominant magnetic interactions, giving impetus for the search for novel frustrated systems, most often based on antiferromagnetic correlations between magnetic ions decorating triangular or tetrahedral lattices. We report here low-temperature magnetic susceptibility and muon spin relaxation results on Li_4MgOsO_6 and $Li_3Mg_2OsO_6$, members of the A_5BO_6 rock-salt ordered family of frustrated materials. In $Li_3Mg_2OsO_6$ we find spin freezing below 12 K. In Li_4MgOsO_6, which can crystallize into either orthorhombic $Fddd$ or monoclinic $C2/m$ crystal symmetries depending on synthesis conditions, we find magnetism consistent with glassylike behavior dominating below 2 K, with partial ordering and evidence for dynamics at somewhat higher temperatures.

DOI: 10.1103/PhysRevB.98.184401

I. INTRODUCTION

Antiferromagnetic (AFM) materials whose magnetic cations comprise triangular or tetrahedral sublattices are unable to satisfy spin correlation constraints simultaneously, resulting in a phenomenon known as geometric magnetic frustration (GMF). In GMF systems the ground states are highly degenerate, which gives rise to rich magnetic phase diagrams exquisitely sensitive to external parameters that make them interesting topics among the condensed matter physics community [1,2]. In systems exhibiting GMF the degree of frustration may be quantified by the frustration index, $f = |\Theta_W|/T_{N/f}$, where Θ_W is the Weiss temperature and T_N or T_f are either the Néel temperatures for long-range magnetic order or the spin-freezing temperatures, respectively [3].

While this phenomenon has been extensively studied in transition-metal oxides with the pyrochlore structure [4], more recently a great deal of attention has been devoted to systems with face-centered cubic (fcc) coordination of magnetic ions, namely ordered NaCl structure-type systems and B-site ordered double perovskites [5,6]. Among the rock-salt-type oxides, materials with the A_5BO_6 general formula have been the center of attention in our research program. Here, A is a diamagnetic ion and B is a paramagnetic heavy ($4d$ or $5d$) transition-metal ion. These systems are particularly interesting as the selected B ions may appear in various oxidation states, enabling a systematic study of the nature of magnetic ground state as a function of spin quantum numbers. In addition, high-Z magnetic ions exhibit a moderate to high degree of spin-orbit coupling, which has been found to result in exotic physics in double perovskites [7–13] and other frustrated systems. Furthermore, these systems crystallize in several different crystal settings, which also provide benchmark examples for the study of structure-property relationships. A_5BO_6 systems are most often found in two crystal systems, namely monoclinic ($C2/m$) and orthorhombic ($Fddd$).

We have discovered and characterized several new members of this family with B = Ru, Re, and Os. $Li_3Mg_2RuO_6$ [14] with Ru^{5+} ($S = 3/2$) ions was the first magnetic member of the family, which was shown to crystallize in the orthorhombic space group, $Fddd$. This compound undergoes a long-range order AFM transition at ∼17 K, which was further confirmed by a λ-shape anomaly in the heat capacity data as well as with temperature-dependent neutron diffraction data. It showed rather mild frustration with $f \sim 6$. Subsequently, its osmate analog $Li_3Mg_2OsO_6$ was synthesized and studied [15]. The latter isoelectronic and isostructural Os-base compound behaved strikingly differently from its ruthenate analog. While a sharp peak in magnetic susceptibility data at ∼8 K without any major divergence between zero-field-cooled (ZFC) and field-cooled (FC) conditions was indicative of long-range order, temperature-dependent heat capacity data revealed a very broad anomaly. This compound exhibits a relatively high frustration index of ∼13. Furthermore, there were

*Corresponding author: jeremy.carlo@villanova.edu
†Corresponding author: shahab.derakhshan@csulb.edu

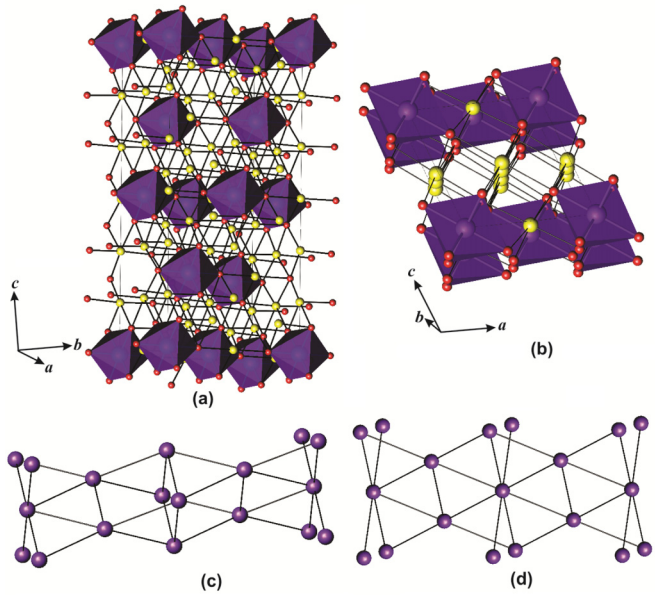

FIG. 1. (a)–(b) Crystal structures of (a) orthorhombic Li_4MgOsO_6, and (b) monoclinic Li_4MgOsO_6. The OsO_6^{6-} octahedra are represented in purple, and the yellow spheres represent the diamagnetic ions (Li^+/Mg^{2+}). The red spheres are O^{2-} ions. (c)–(d) The magnetic sublattices of (c) orthorhombic and that of (d) monoclinic Li_4MgOsO_6. The purple spheres represent Os^{6+} and the black lines indicate magnetic exchange pathways between the nearest neighbors.

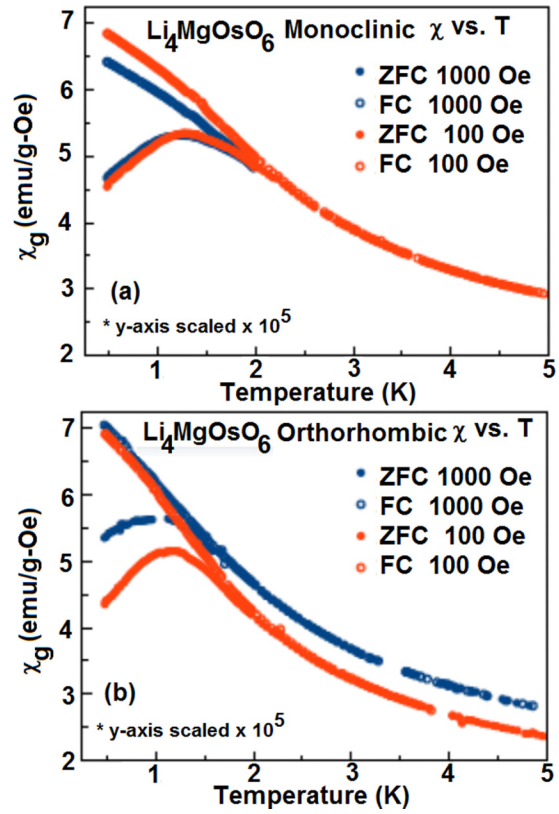

FIG. 2. Temperature-dependent zero-field cooled/field cooled (ZFC, FC) magnetic susceptibility data for (a) monoclinic Li_4MgOsO_6 and (b) orthorhombic Li_4MgOsO_6 under applied magnetic fields of 100 Oe (red) and 1000 Oe (blue).

no magnetic neutron diffraction peaks down to 4 K. Hence, the nature of the magnetic ground state of $Li_3Mg_2OsO_6$ has remained uncertain.

Most recently, we were able to synthesize the $S = 1$ members of the family (Li_4MgOsO_6) in two different crystal settings, monoclinic $C2/m$ and orthorhombic $Fddd$ [16]. The crystal structures of the two polymorphs are presented in Figs. 1(a) and 1(b). The major difference between the arrangement of magnetic ions in these two systems lies in their dimensionality. While the orthorhombic lattice is composed of both two-dimensional (2D) edge-sharing triangles and 3D structures resembling wedges [Fig. 1(c)], the monoclinic phase comprises an edge-sharing triangular sublattice in a 2D fashion [Fig. 2(d)]. Nevertheless, the static magnetism in these two polymorphs were shown to be very similar. Both compounds showed no evidence of magnetic transition in temperature-dependent magnetic susceptibility data down to 2 K. The Curie-Weiss fits to the paramagnetic regime resulted in large, negative, and very similar Weiss constants (−115 K and −122 K for monoclinic and orthorhombic phases, respectively) indicating predominant AFM exchange correlations; the lack of a transition down to 2 K indicates that both systems are highly frustrated ($f > 50$).

However, it should be noted that Θ_W can be sensitive to the temperature range over which it is measured, and ordering temperature can be suppressed through mechanisms other than frustration, thus f can be influenced by factors besides geometric frustration. Nonetheless, it is a useful rough metric for comparison of closely related specimens, although further study is required to confirm magnetic behavior. Therefore, to better understand the ground-state magnetic properties of these specimens, we report on low-temperature magnetic susceptibility and magnetic relaxation data for both phases of Li_4MgOsO_6 as well as μSR data for $Li_3Mg_2OsO_6$ and both Li_4MgOsO_6 phases.

II. EXPERIMENTAL

Synthesis. Nearly one gram samples of orthorhombic $Li_3Mg_2OsO_6$, orthorhombic Li_4MgOsO_6 and monoclinic Li_4MgOsO_6 were prepared by high-temperature solid-state techniques. Details of these syntheses were explained in our previous reports [15,17].

Phase analyses. To examine the formation and ensure the purity of produced phases, powder x-ray diffraction was employed. Data were collected using a PANalytical X′Pert Pro MPD diffractometer, equipped with a linear X′ Celerator detector, with Cu-Kα_1 radiation.

Magnetic susceptibility measurements. ZFC and FC low-temperature susceptibility data were collected for both Li_4MgOsO_6 phases using a Quantum Design MPMS SQUID magnetometer equipped with an IQuantum ^{3}He insert with a base temperature of 0.48 K, under applied magnetic fields of 100 and 1000 Oe.

Magnetization relaxation measurements. Since the previously studied static magnetic properties were almost identical for both Li_4MgOsO_6 phases, temperature-dependent

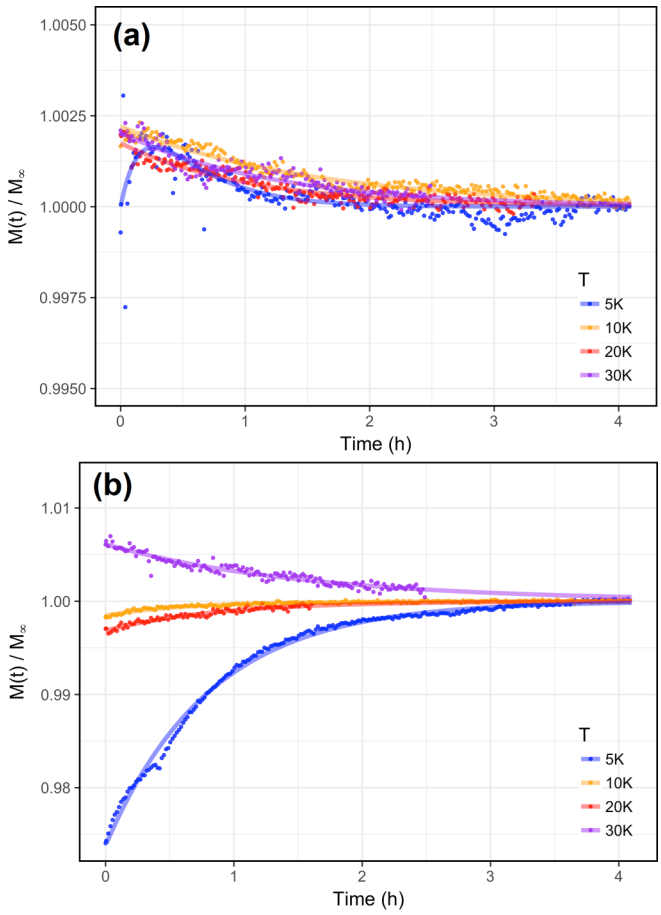

FIG. 3. The time-dependent magnetization $M(t)$ measured at four different temperatures in an applied field of 0.1 T for (a) the monoclinic phase, and (b) the orthorhombic phase, using a vibrating sample magnetometer. The data is normalized to the asymptotic magnetization value M_∞ for comparison at different temperatures. The solid lines are fits to a single exponential function, and a double exponential for $T = 5$ K.

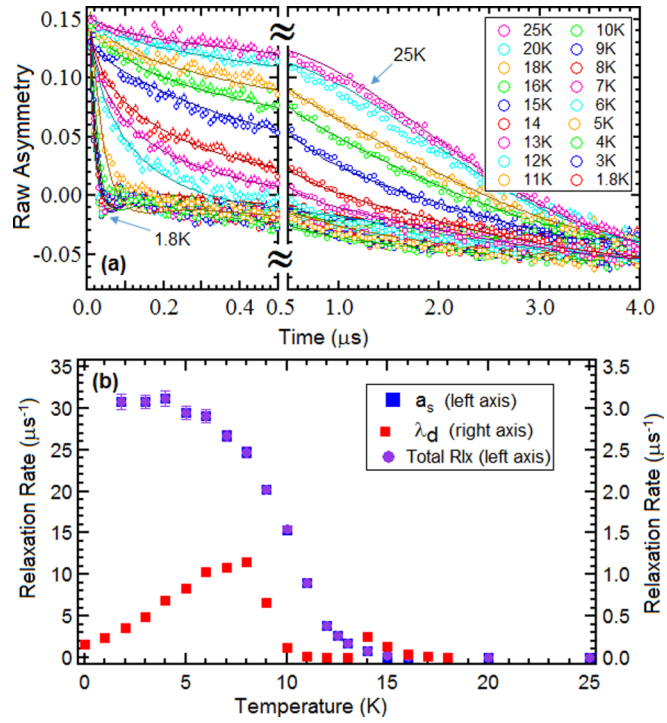

FIG. 4. (a) Muon spin relaxation data for $Li_3Mg_2OsO_6$, fitted to the Uemura spin glass function as described in the text. The short-time and long-time domains are shown with separate scaling to emphasize both the rapid initial relaxation and the slower long-time behavior. For clarity, the highest and lowest temperature traces are individually labeled. (b) Fits to the Uemura spin glass function of muon spin relaxation data for $Li_3Mg_2OsO_6$, exhibiting an onset of magnetic order below 12 K. For clarity, a_s and total relaxation $\sqrt{a_s^2 + \lambda_d^2}$ are scaled by the left y axis, while λ_d uses the right y axis.

magnetic relaxation data collections were performed with a Quantum Design PPMS vibrating sample magnetometer. For this purpose, samples were cooled down under zero field to the measurement temperature. A magnetic field of 0.1 T was then applied and the time-dependent magnetization was measured for 5–30 ks at $T = 5$ K, 10 K, 20 K, and 30 K for both samples.

Muon spin relaxation spectroscopy. To further characterize the magnetic ground state, muon spin relaxation (μSR) measurements were performed. Muon spin relaxation is particularly useful in elucidating magnetic behavior in specimens with low-moment and/or spatially disordered magnetism, as are frequently encountered in geometrically frustrated systems, and can distinguish the effects of static order from dynamically fluctuating spins in systems exhibiting spin freezing. In a μSR experiment, spin-polarized muons are implanted one at a time into a sample, within which each undergoes Larmor precession due to local magnetic fields at the implantation site. The muons decay with a characteristic timescale of 2.2 μs, and emit positrons preferentially along the instantaneous spin axis of the muon at time of decay. The time and directional dependence of the positron emission can thus be used to reconstruct the time-dependent muon spin polarization function $G_z(t)$, from which the internal field distribution may be deduced. The decay positrons are detected by a pair of counters on opposite sides of the sample, with the asymmetry defined as the difference between the count rates in the two detectors divided by the sum. Note that due to differing detector efficiencies and geometry, the baseline raw asymmetry (corresponding to zero net muon spin polarization) can be different from zero. Measurements were conducted at TRIUMF (Vancouver, BC) using the M20 beam line with 4.2 MeV surface muons and the LAMPF spectrometer at temperatures from 2–125 K, in both zero-field (ZF) and longitudinal-field (LF) configurations.

III. RESULTS AND DISCUSSION

Low-temperature ZFC and FC SQUID data are shown for the monoclinic and orthorhombic Li_4MgOsO_6 phases in Figs. 2(a) and 2(b), respectively. Clear AFM-type transitions are observed for both $C2/m$ and $Fddd$ phases at 1.5 K and 1.3 K, respectively, corresponding to frustration indices $f = 77$ and 94. Such divergence is indicative of spin-glass behavior for both samples, with a slightly lower transition temperature in the orthorhombic phase as compared to the

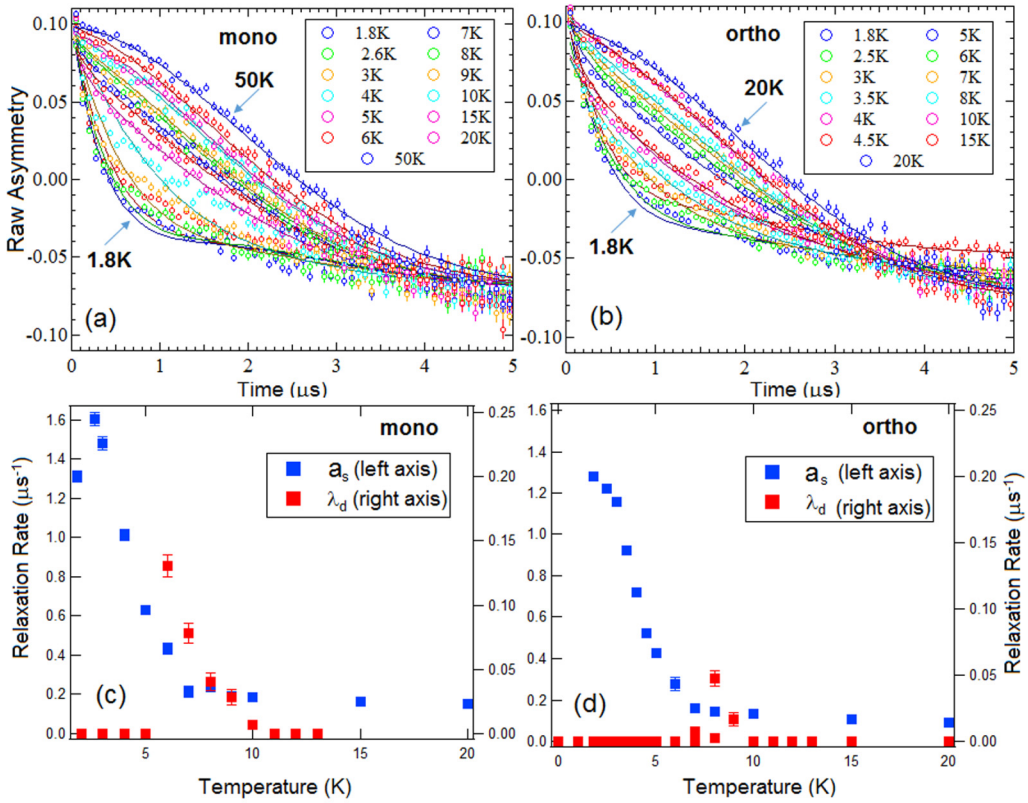

FIG. 5. (a)–(b) Muon spin relaxation data for Li_4MgOsO_6, fitted to the Uemura spin glass function as described in the text; the monoclinic specimen is shown at (a) left, with the orthorhombic specimen at (b) right. For clarity, the highest and lowest temperature traces are labeled individually. (c)–(d) Fits to the Uemura spin-glass function for (c) monoclinic and (d) orthorhombic Li_4MgOsO_6. Both exhibit onset of relaxation just above 5 K, and become fully ordered at a temperature below 2 K.

monoclinic. The spin-glass magnetic ground state is also consistent with the cationic occupancy disorder between Li and Mg ions in crystallographic cationic position [18].

Both phases of Li_4MgOsO_6 show slow magnetic relaxation, albeit with different long-term behavior, as shown in Fig. 3. The magnetization is measured after a magnetic field of 0.1 T is established and increases in magnitude for lower temperatures. For easier comparison, the magnetization $M(t)$ is normalized to the asymptotic magnetization value M_∞, which is obtained from a single exponential fit to the experimental data. In the case of the monoclinic phase, the magnetic relaxation is more pronounced. While at 5, 10, and 20 K the magnetization is still increasing over time, at 30 K the opposite trend is observed. At the lowest temperatures, the sweep field speed of 100 Oe per second is faster than the sample response time, so that the magnetization is increasing in response to the applied field, whereas it is likely an aging effect gives rise to the magnetization decrease at higher temperatures. All data can be fit to a single exponential with a typical time constant of around 3000 s. These fits are shown as solid lines in Fig. 3. In the case of the orthorhombic phase, there is a decrease for all temperatures, except at the lowest measured temperature of 5 K, in which case a double exponential is used to capture both the initial increase that is then followed by the relaxation of the magnetization. This slow magnetic relaxation is characteristic of glassy systems.

The zero-field μSR data for $Li_3Mg_2OsO_6$ are shown in Fig. 4(a), evidencing an onset of relaxation below 12 K, consistent with glassy-type ordering. These data were fitted to the Uemura spin glass function [19], which was developed for dilute magnetic alloys but has been used more generally for frustrated small-moment systems exhibiting glassy or spatially complex magnetism:

$$G_z(t) = \frac{1}{3}\exp(-\sqrt{\lambda_d t}) + \frac{2}{3}\left(1-\frac{a_s^2 t^2}{\sqrt{\lambda_d t + a_s^2 t^2}}\right)\exp\left(-\sqrt{\lambda_d t + a_s^2 t^2}\right). \quad (1)$$

Here, a_s represents the statically ordered moment, while λ_d represents relaxation due to dynamically fluctuating moments. The 2/3 term corresponds to the component of magnetic moments perpendicular to the initial muon spin asymmetry, which are relaxed by both the static and dynamic components of magnetism, whereas the 1/3 term represents the component parallel to the initial muon spin asymmetry, which is only relaxed by dynamically fluctuating moments. Fits to the Uemura spin glass function are shown in Fig. 4(b), exhibiting an onset of static relaxation starting just above 12 K, with dynamical fluctuations peaking somewhat below 10 K. The rise in a_s and the peak in λ_d are consistent with a progressive slowing down

of spin fluctuations, resulting in static order at base temperature. Since the 1/3 and 2/3 terms have similar functional forms and can exhibit significant interplay in fitting, a total relaxation equal to $\sqrt{\lambda_d^2 + a_s^2}$ is also shown and exhibits an order-parameter-like dependence with onset at 12 K with the relaxation at base temperature approaching 31 μs^{-1}. It should be noted the slow relaxation evident at higher temperatures (e.g., 25 K) is due to nuclear dipolar relaxation from the large Li nuclear moments.

μSR data for both crystal settings of Li_4MgOsO_6 are shown in Figs. 5(a) and 5(b). Both specimens exhibit onset of low-temperature relaxation, albeit at a temperature scale approximately half as high as in $Li_3Mg_2OsO_6$, and with low-temperature relaxation rates about 20 times smaller, corresponding to a commensurately smaller ordered moment size. These data were also fitted to the Uemura spin-glass function, as shown in Figs. 5(c)–5(d). In both cases the static moment a_s exhibits order-parameter-like dependence commencing at around 5 K, while dynamical relaxation λ_d exhibits a peak and then declines toward zero as the fluctuations slow down through the muon's characteristic time window.

In both specimens, relaxation becomes apparent at around 5 K, although full order does not appear to set in until 2 K or below, consistent with the low-temperature susceptibility measurements. As with $Li_3Mg_2OsO_6$, the high-temperature relaxation is due to Li nuclear dipolar moments. The relaxation rates at base temperature are 1.6 μs^{-1} in the monoclinic specimen and 1.3 μs^{-1} in the orthorhombic setting. This corresponds to a 20–25% larger ordered moment size in the monoclinic specimen, commensurate with the observed ratio of ordering temperatures.

IV. CONCLUSIONS

We have studied the rock-salt ordered antiferromagnets $Li_3Mg_2OsO_6$ and Li_4MgOsO_6 in the context of geometric magnetic frustration. These systems most often crystallize into either orthorhombic $Fddd$ or monoclinic $C2/m$ crystal settings; Li_4MgOsO_6 in particular can crystallize into either of these crystal settings depending on synthesis conditions, making its study especially valuable in elucidating ground-state determination in rock-salt ordered systems. $Li_3Mg_2OsO_6$ and both crystal settings of Li_4MgOsO_6 are observed to exhibit magnetic ordering consistent with spin freezing, with dynamical slowing down of fluctuations observed while crossing through the transition. In $Li_3Mg_2OsO_6$, the spin-freezing temperature indicated by muon spin relaxation is 12 K. While in both specimens of Li_4MgOsO_6 the onset of relaxation in μSR data occurs around 5 K, low-temperature magnetic susceptibility measurements indicate an ordering temperature in both of 1.5 K in the monoclinic specimen and 1.3 K in the orthorhombic specimen, corresponding to high frustration indices of 77 and 94, respectively. The ordered moment size and the ordering temperature in monoclinic Li_4MgOsO_6 is about 20% larger than in its orthorhombic polymorph, highlighting the significance to ground-state determination of subtle structural distortions and differing magnetic pathways, as depicted in Fig. 1. The ordered moment size in the $5d^3$ $Li_3Mg_2OsO_6$ is about 20 times larger than the moment size in either specimen of $5d^2Li_4MgOsO_6$, although the fully ordered moment size may not be achieved by the lowest temperature (1.8 K) accessible to the muon spin relaxation experiments.

ACKNOWLEDGMENTS

S.D. is grateful for financial support from NSF-DMR-RUI Award No. 1601811. S.D. and T.G. also acknowledge support from W. M. Keck Foundation for establishment of the Keck Energy Materials Program at CSULB. J.P.C. acknowledges support from the Research Corporation for Science Advancement (Cottrell College Science Award No. 23314). We thank the TRIUMF CMMS for assistance with μSR experiments.

[1] J. E. Greedan, J. Mater. Chem. **11**, 37 (2001).
[2] L. Balents, Nature (London) **464**, 199 (2010).
[3] P. Schiffer and A. P. Ramirez, Comments Cond. Mat. Phys. **18**, 21 (1996).
[4] J. S. Gardner, M. J. P. Gingras, and J. E. Greedan, Rev. Mod. Phys. **82**, 53 (2010).
[5] C. J. Howard, B. J. Kennedy, and P. M. Woodward, Acta Cryst. B **59**, 463 (2003).
[6] M. T. Anderson, K. B. Greenwood, G. A. Taylor, and K. R. Poeppelmeier, Prog. Solid St. Chem. **22**, 197 (1993).
[7] C. M. Thompson, C. A. Marjerrison, A. Z. Sharma, C. R. Wiebe, D. D. Maharaj, G. Sala, R. Flacau, A. M. Hallas, Y. Cai, B. D. Gaulin, G. M. Luke, and J. E. Greedan, Phys. Rev. B **93**, 014431 (2016).
[8] D. D. Russell, A. J. Neer, B. C. Melot, and S. Derakhshan, Inorg. Chem. **55**, 2240 (2016).
[9] S. Gangopadhyay and W. E. Pickett, Phys. Rev. B **91**, 045133 (2015).
[10] A. E. Taylor, R. Morrow, D. J. Singh, S. Calder, M. D. Lumsden, P. M. Woodward, and A. D. Christianson, Phys. Rev. B **91**, 100406(R) (2015).
[11] A. Sarapulova, P. Adler, W. Schnelle, D. Mikhailova, C. Felser, L. H. Tjeng, and M. Jansen, Z. Anorg. Allg. Chem. **641**, 769 (2015).
[12] Y. Yuan, H. L. Feng, M. P. Ghimire, Y. Matsushita, Y. Tsujimoto, J. He, M. Tanaka, Y. Katsuya, and K. Yamaura, Inorg. Chem. **54**, 3422 (2015).
[13] G. Chen, R. Pereira, and L. Balents, Phys. Rev. B **82**, 174440 (2010).
[14] S. Derakhshan, J. E. Greedan, T. Kastumata, and L. M. D. Cranswick, Chem. Mater. **20**, 5714 (2008).
[15] P.-H. T. Nguyen, F. Ramezanipour, J. E. Greedan, L. M. D. Cranswick, and S. Derakhshan, Inorg. Chem. Mater. **51**, 11493 (2012).
[16] P.-H. T. Nguyen, M. C. Kemei, M. S. Tan, and S. Derakhshan, J. Solid State Chem. **242**, 155 (2016).

[17] S. Derakhshan, J. E. Greedan, and L. M. D. Cranswick, Phys. Rev. B. **77**, 014408 (2008).

[18] E. A. Zvereva, I. A. Presniakov, M.-H. Whangbo, H.-J. Koo, T. V. Frantsuzenko, O. A. Savelieva, A. V. Sobolev, V. B. Nalbandyan, P.-S. Shih, J.-C. Chiang, J.-M. Lee, J.-M. Chen, J.-Y. Lin, B. Büchner, and A. N. Vasiliev, Appl. Magn. Reson. **46**, 1121 (2015).

[19] Y. J. Uemura, T. Yamazaki, D. R. Harshman, M. Senba, and E. J. Ansaldo, Phys. Rev. B **31**, 546 (1985).